Hindawi
Advances in Civil Engineering
Volume 2023, Article ID 5587275, 17 pages
https://doi.org/10.1155/2023/5587275

Research Article

On the Responses of Braced Diaphragm Wall Supporting Deep Excavation Subjected to Asymmetric Surcharge Loads

Recep Akan

Department of Civil Engineering, Faculty of Engineering, Suleyman Demirel University, Isparta 32200, Turkey

Correspondence should be addressed to Recep Akan; recepakan@sdu.edu.tr

Received 6 June 2023; Revised 13 July 2023; Accepted 3 September 2023; Published 3 October 2023

Academic Editor: Luigi Fenu

As cities grow, so does the need for housing and transportation infrastructure, necessitating deep excavations. Near the deep excavation, especially in the urban centers, there are existing structures whose loads are often different, resulting in asymmetric loading of the excavation system and different behavior on each side of the excavation. In this study the strut forces, lateral deformations, bending moments on each wall, as well as the settlements and heaves of the soil behind both walls in the asymmetrically loaded strut-supported excavation system are determined using the finite element method (FEM). The analyzes are performed using Plaxis 2D v20, a computer software based on the FEM. In addition, regression analyses are performed on the results, and correlations that predict the relevant results depending on the surcharge loads are presented.

1. Introduction

With the increasing population in recent years, high-rise buildings have been needed, especially in the city centers. With the increasing need for public transportation, subways have also become more prevalent. Deep excavations are a prerequisite for structures such as high-rise buildings and subway stations. Deep excavations must be supported so that they do not damage adjacent structures, ensure their safety and reduce the deformations. Many studies in the literature examine the deformations of the walls and surface soil and the loads on the struts and anchors in the deep excavations. Bransby and Milligan [1] established a laboratory model to determine the deformations in the soil near the cantilever sheet pile wall on dry sandy soil and presented an analytical method showing a relationship between the deformations at the soil surface and the displacements at the wall. Ou et al. [2] analyzed the case studies and showed the location and relationships between the maximum horizontal wall deformation and maximum soil surface settlement. They also proposed an empirical formula for determining the profile of soil surface settlement. In addition, Clough and O'Rouke [3] evaluated wall movements on site-built walls due to excavation, shoring, and auxiliary work separately from field observations and introduced a new understanding of modeling excavation problems using the finite element method (FEM). Cheng et al. [4] developed a simplified analytical method using the theory of elasticity to determine the ground lateral displacement resulting from foundation pit excavation and validate the outcomes of the suggested analytical solution by contrasting them with well-documented field data. Additionally, they perform a parametric analysis to identify the variables that most significantly influence ground lateral displacement. Wong and Goh [5] studied the effect of cracks in the wall on the behavior of the wall during top–down excavation and they found that the crack in the wall significantly reduced the bending moment but slightly increased the lateral displacement.

Subsequently, some researchers conducted finite element analyses to model the experimental models [6, 7] and case studies and field observations [5, 8–10] to calculate the soil surface settlement, horizontal displacements of the wall, and soil stresses. Ghobrial et al. [11] determined the lateral earth pressures by modeling the excavation with the FEM and found that the results were compatible with the apparent pressure diagrams developed by Peck [12] and Tschebotarioff [13]. Hsu et al. [14] calculated soil stresses occurring during the excavation in gravel soils using analytical methods

[12, 13, 15] and compared them with data obtained from the case studies. With the development of computer technology, many researchers have carried out parametric studies to investigate the vertical deformations that will occur in sandy soils and the change in wall deformations and soil pressure using the 2D FEM and finite difference method. In these studies, parameters such as sand density, excavation depth and width, wall length and stiffness, and pier stiffness and spacing were considered by performing the analysis using computer-based software such as Plaxis 2D v20, Midas Gtx, Abaqus [16–26].

Hsiung et al. [27] analyzed wall movements, and Chheng and Likitlersuang [28] additionally analyzed soil surface settlements using the 3D FEM, compared them with field measurements, and found that the results were reasonable and reliable. Goh et al. [29] performed both 2D and 3D finite element analyses and showed that the 3D analyses yielded lower wall deformations and proposed an equation for estimating the maximum wall deformation. Zhang et al. [30] performed both 2D and 3D finite element analyses for dense sand and gravel soils and a medium-rigid wall, and claimed that current studies in the literature did not address these soil types much. The results obtained were compatible with the field measurements, and a correlation was proposed to determine the strut force based on the parametric study results. Goh and Wong [31] performed a 3D finite element analysis to study the load change in the adjacent struts when one or two struts fail and found that transfers its load to the adjacent struts, and the bending moment on the wall does not change significantly. In addition, Pong et al. [32] proposed a procedure to optimize the strut forces determined by the 2D analyses according to the results of the 3D analyses in the case of failure of a single strut because the 2D analyses require more time than the 3D analyses. Some researchers study soft soils using the numerical methods and computer-based software.

Although there are buildings and roadways close to the deep excavations, particularly in the city center and it is more likely that the surcharge loads are asymmetrical, the excavations are typically modeled using a half-model assuming the loads are symmetrical. However, the strut forces, the walls' behavior and the soil surface's settlements changes because each wall responds to asymmetic loading in different way hazardous and unprofiteable results may be caused. By carefully analyzing and designing the walls, it is feasible to get rid of the hazardous conditions and find a cost-effective solution. Wu [33] performed a simplified and limited analysis using Winkler's model for the case of asymmetric surcharge load. In addition, Xu et al. [34] and Guo et al. [35] performed a finite element analysis and finite difference analysis, respectively, and found that the presence of surcharge loads on both sides of the excavation has different magnitudes, resulting in different lateral deformations and bending moments for both walls and that the asymmetry negatively affects the support system of the excavation. Zhang et al. [36] used a numerical simulation of stage excavation to study the excavation of a subway station next to a river and a main road. The asymmetrical pressure of the excavation induced by the distance between the external load and excavation is studied using parameter analysis. The findings show that asymmetrical pressure on the excavation is significant and cannot be ignored if there is a river channel and an external load within the excavation depth range. The influence of asymmetrical pressure can be reduced, and the stability of adjacent riverside layers may be enhanced by increasing the stiffness of the diaphragm wall. There are very few studies on this topic in the literature so far, so further studies on this topic will contribute to the literature.

Diaphragm walls are strong concrete structures that are framed panel by panel. Diaphragms are typically made of concrete slabs for concrete structures or metal or composite metal decks for steel structures. Diaphragm walls are mostly employed near existing structures when the earth and depth would make piled walls difficult. Diaphragm walls are simple and inexpensive to construct and available worldwide. Tunnels, deep basements, underpasses, underground car parks, and railway stations are some of the most popular applications. It has three main types flexible, rigid, and semirigid diaphragms. Flexible diaphragms withstand lateral forces based on the tributary area, regardless of the flexibility of the parts to which they transfer force. Rigid diaphragms transfer the load to frames or shear walls depending on their flexibility and position in the structure. The flexibility of a diaphragm influences the distribution of lateral forces to the vertical components of a structure's lateral force-resisting parts.

The present study aims to investigate the change in strut loads, deformations, and bending moments on the diaphragm walls, ground surface settlements, and heave in the strut-supported deep excavations under asymmetric surcharge loads. In this context, strut-supported deep excavation systems have diaphragm walls in loose (LS) and dense (DS) sandy soils are modeled for various loading scenarios using PLAXIS 2D v20 [37], a finite element-based computer program. Parametric analyses are first performed to determine the effects of model boundaries (X, Y), mesh size, wall-soil interface strength reduction (Rinter), the width of the pit (B), embedment depth (Df), and thickness (d) of the walls to determine ascertain the main model for the study. Then, a comprehensive parametric study covering the symmetric and asymmetric surcharge load scenarios for LS and DS is carried out and the results are presented in tables and illustrated in figures. In addition, linear and polynomial second-order relationships are obtained using the SPSS Statistics v17 computer program to estimate the maximum values of the strut forces (Tst), the deformations (UxL and UxR) and bending moments (ML and MR) on the diaphragm walls, the ground surface settlements (UyL and UyR) for both the left and right sides of the excavation and the heaves (Hv) in the excavation as a function of the surcharge situations on both sides of the excavation.

2. Materials and Methods

2.1. Finite Element Method. It is difficult to solve the geotechnical correlations because there are so many factors involved, including strain, stress, shear pressures, deflections, and

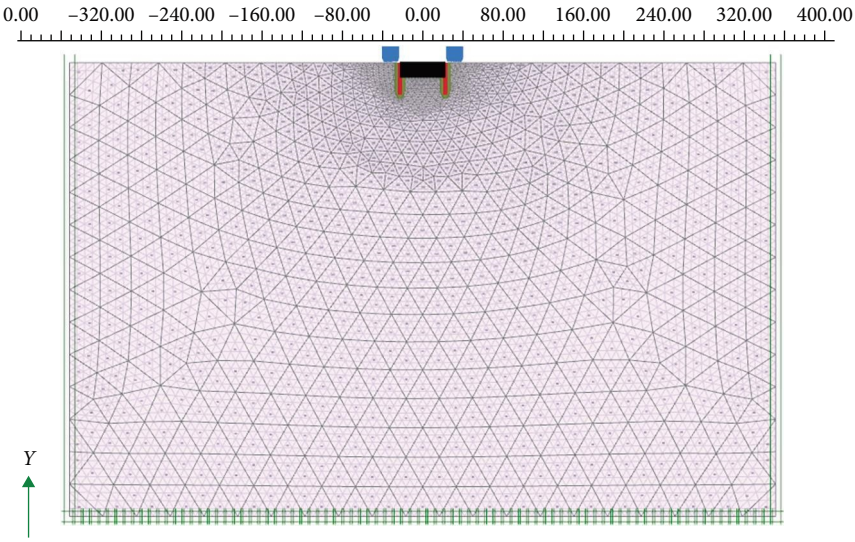

Figure 1: Meshed finite element model of the deep excavation.

bending moments, makes it complicated. Because of this, numerical modeling is a crucial tool for streamlining and improving the accuracy of complex calculations. The FEM is a technique for finding solutions to engineering problems by assembling the variables into vectors and matrices in computer programs and solving the system numerically. These challenging solution processes can be easily solved using a variety of technologies, including the Plaxis program used in the study. The current study employs a two-dimensional FE model considers plane strain model, and the excavation models are modeled as a whole for symmetric and a symmetric loading scenarios. The effects of mesh size on the behavior of the excavation support system are minimized by using a "fine mesh." The "fine" option from the program's settings was used to generate the mesh networks depicted in Figure 1. There are 1,942 soil elements and 16,055 nodes in the linked mesh network. There are two diaphragm walls, one on the left and one on the right side of the excavation, simulated with a five-noded elastic plate and connected to the surrounding soil by an interface element. The parameters of the walls and struts are taken from Xu et al. [34]. In addition, the wall's area and moments of inertia are changed so that the elastic modulus remains constant to study the behavior of the walls at different thicknesses. The boundary conditions allow vertical movement of the sides and the vertical and horizontal movement of the upper boundary, while no movement is permitted at the lower boundary. The horizontal boundaries are 350 m from the center of the excavation on both sides, and the lower boundary is 350 m below the ground surface to avoid the negative effects of the model boundaries. The struts are modeled with a "node-to-node anchor" at 3-m horizontal and vertical intervals. The parameters of the excavation shoring system are given in Table 1.

Excavation and wall's embedment depths are both assumed to be 16 m, the support system is designed with five struts, and groundwater is not considered. In the analysis, the loading type "staged construction" is chosen. The excavation is carried out

Table 1: Parameters of excavation support system.

Parameters	Diaphragm walls			Struts
Thickness, d (cm)	40	80	120	–
Material type	Elastic	Elastic	Elastic	Elastic
EA (kN/m)	24×10^6	48×10^6	72×10^6	2×10^6
EI (kNm^2/m)	320×10^3	256×10^4	864×10^4	–
ν	0.15	0.15	0.15	–

in eight stages, and the applied construction phases are shown in Table 2.

Each excavation is made to a depth of 1 m below the next bracing level, and the corresponding strut is activated in the next stage. The schematic model of the five-stage bracing system, diaphragm walls and surcharge loads is shown in Figure 2.

2.2. Constitutive Model. In the present work, LS and DS are used as soil materials and the hardening soil model is adopted, which takes into account the friction-induced swelling behavior in soil and allows modeling under the triaxial volume deformation conditions, where the Mohr–Coulomb failure criterion defines failure. The hardening soil parameters used in the study are taken from the studies of Brinkgreve et al. [38] and Xuan [39] and are listed in Table 3.

3. Results and Discussion

3.1. The Validation of the Model. Problems of the three research provided in the literature are modeled using Plaxis 2D v20 and the results are compared to the results presented in the relevant paper for validation. The strut forces from Zhang et al. [30] are compared in Figure 3, the ground surface settlements from Mohamed et al. [24] are compared in Figure 4, and the wall deflections for flexible and stiff walls from Goh et al. [40] are compared to the results of current models in Figure 5.

Table 2: Construction procedure for 2D analysis.

Phase	Construction
1	Initial phase
2	Install the walls and surcharge loads
3	Excavate till the 1st excavation level (−2 m)
4	Install 1st strut (S1) at −1 m and excavate till the 2nd excavation level (−5 m)
5	Install 2nd strut (S2) at −4 m and excavate till the 3rd excavation level (−8 m)
6	Install 3rd strut (S3) at −7 m and excavate till the 4th excavation level (−11 m)
7	Install 4th strut (S4) at −10 m and excavate till the 5th excavation level (−14 m)
8	Install 5th strut (S5) at −13 m and excavate till the 5th excavation level (−16 m)

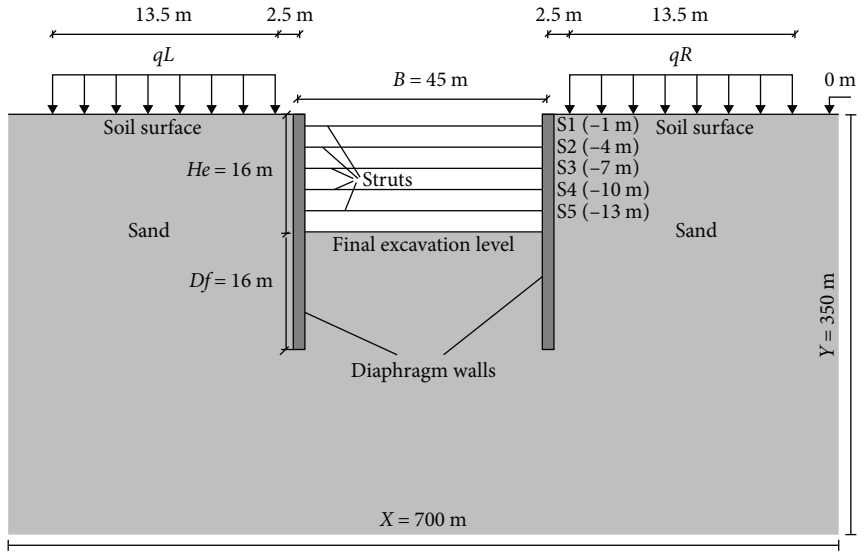

Figure 2: Scheme of the model for supported excavation system.

Table 3: The hardening soil parameters of LS and DS.

Parameters	DS	LS	Parameters	DS	LS
Yunsat (kN/m^3)	18.2	17	$\varphi(^\circ)$	38	30
Ysat (kN/m^3)	20.3	19	$\Psi(^\circ)$	8	0
Drainage type	Drained	Drained	υ_{ur}	0.35	0.2
$k_x = k_y$ (m/day)	10^{-8}	10^{-8}	p^{ref} (kN/m^2)	100	100
$\sum_{50}^{ref}$ (kN/m^2)	48,000	15,000	m	0.45	0.8
$\sum_{oed}^{ref}$ (kN/m^2)	48,000	15,000	K_0^{nc}	0.3843	0.5
$\sum_{ur}^{ref}$ (kN/m^2)	144,000	45,000	R_f	0.9	0.9
c (kN/m^2)	0	0	R_{inter}	0.4, 0.6, 0.8, 1	0.4, 0.6, 0.8, 1

The results are found to be in fair agreement with slight fluctuation. Many parameters considered when developing the model have an impact on the results and some parameters are not explicitly stated in previous studies that are compared. The modest discrepancies in the results are assumed to be related to this uncertainty.

3.2. The Effects of the Model Parameters. The behavior of the excavation support system changes when the models are built with very fine or very coarse mesh size as well as width or narrow. The model width and mesh size cause time and labor losses and unsafety problem when they are not chosen appropriately so it is necessary and beneficial to determine the optimal model size and mesh size. Parametric studies are carried out to determine the width, depth and mesh size of the model to be used in the analyses where the effects of asymmetric surcharge load are studied, which is the main purpose of the paper. At this stage, it is assumed that a surcharge load of 60 kPa exists on both sides of the excavation, which is the largest surcharge load of this study. Here, UyL,

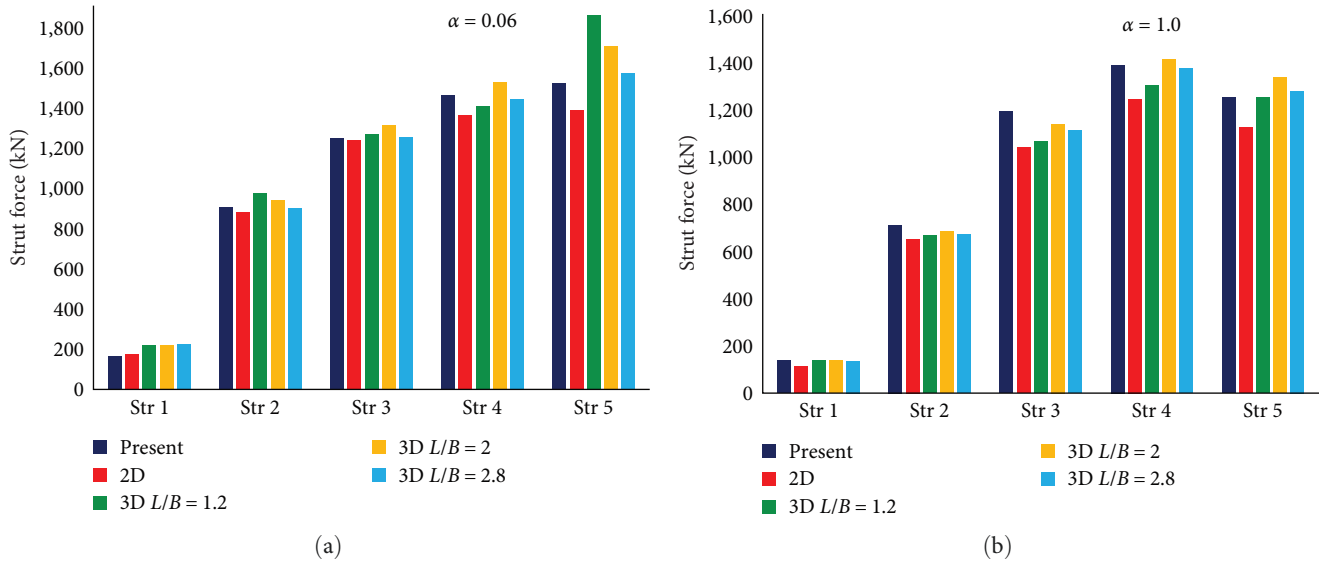

FIGURE 3: The comparison of strut forces from Zhang et al. [30] and the present model for (a) flexible and (b) stiff wall.

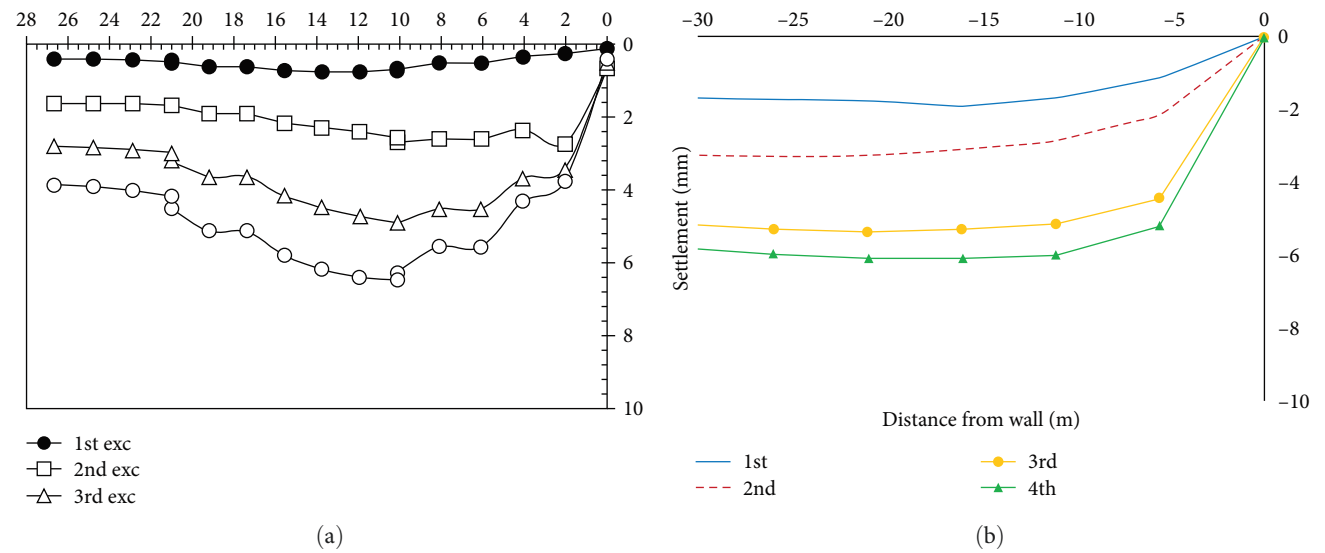

FIGURE 4: Ground surface settlements from (a) Mohamed et al. [24] (b) present model.

UxL, and ML represent the results for the wall on the left side (WL) and the soil behind WL, while UyR, UxL, and MR represent the results for the wall on the right side (WR) and the soil behind WR.

3.3. The Effect of the Boundary Conditions and Mesh Size. Table 4 shows the analysis results performed at different model dimensions for LS and DS considering that the mesh size is fine, Df = 16 m, $d = 40$ cm, $R_{inter} = 0.6$, and $B = 45$ m. Model dimensions are changed to approximately 20 times the excavation width, keeping the ratio of horizontal width (X) to vertical depth (Y) constant. The results include the maximum values for *Tst*, *UyL*, *UxL*, *ML*, and *Hv*.

While the values of *Tst*, *UxL*, and *UyL* hardly change with the change in model dimensions, the values of *UyL* decrease with the increase in model dimensions. Because the model is supported horizontally on both sides against deformation, this condition causes bulging within the impact limits and affects vertical deformation. This change in *UyL* loses its effect after $Y = 500$ m and $X = 250$ m for *DS* and $Y = 700$ m, and $X = 350$ m for *LS*. Therefore, the model dimensions are considered as $Y = 700$ m and $X = 350$ m in the rest of the study.

Table 5 shows the analysis results performed at different mesh sizes, from very coarse to very fine for *LS* and *DS* considering that model dimensions are 700 m horizontally and 350 m vertically, $R_{inter} = 0.6$, $Df = 16$ m, $d = 40$ cm, and $B = 45$ m. The results include the maximum values for *Tst*, *UyL*, *UxL*, *ML*, and *Hv*.

The *Tst* and *Hv* values almost do not change with the change in mesh size. At the same time, *UyL* decreases slightly, and *ML*

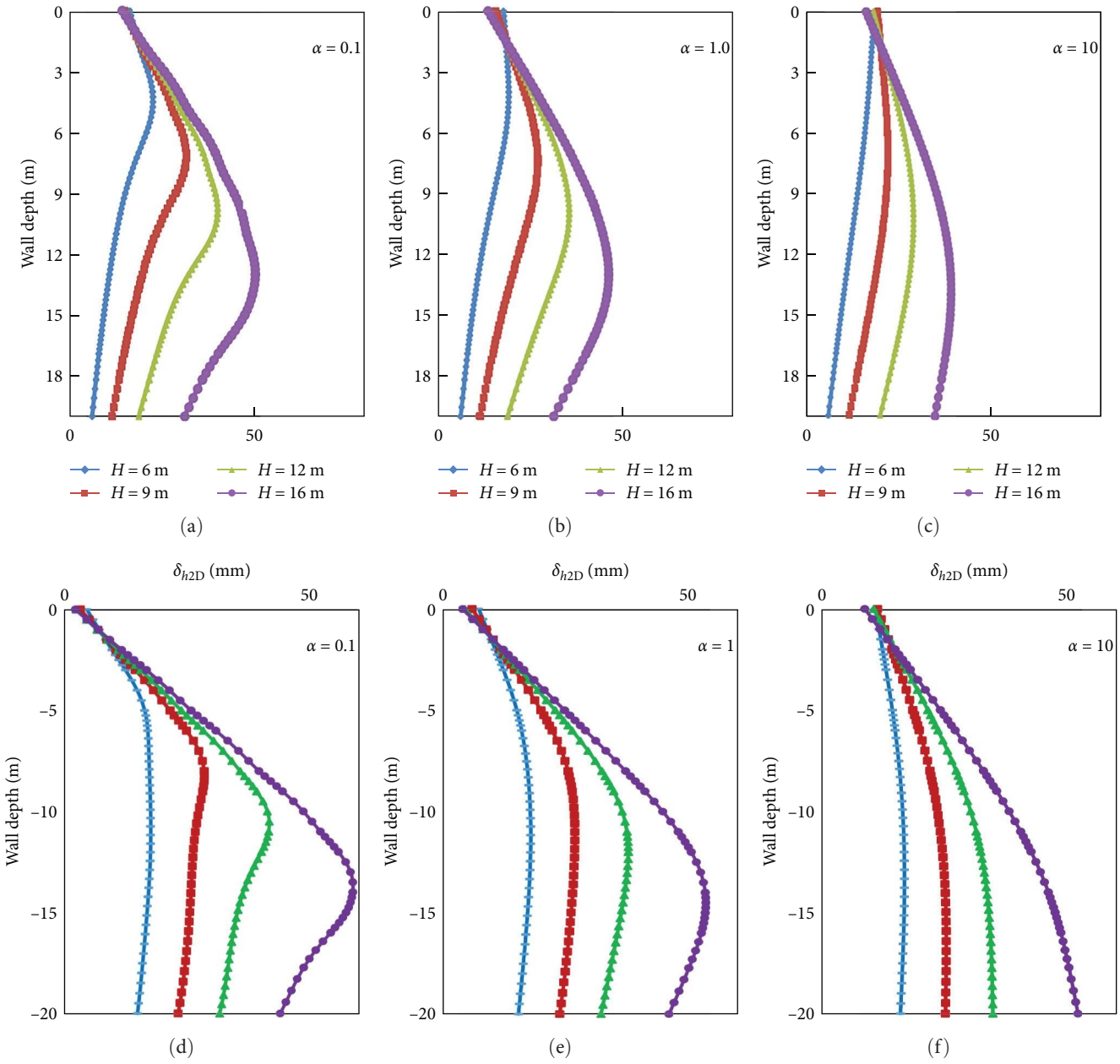

Figure 5: Wall deflection from (a–c) Goh et al. [40] to the (d–f) present model.

increases significantly from very coarse to medium and gradually stabilizes after the medium mesh size, especially in *LS*.

3.4. The Effect of the Thickness and Embedment Depth of the Wall. The effects of wall thickness on the deformation and bending moment of the *WR* as well as the deformations behind the *WR* and at the bottom of the excavation considering that the model size is 700 m horizontally and 350 m vertically and the mesh size is fine, $R_{\text{inter}} = 0.6$, $Df = 16$ m, and $B = 45$ m is shown in Figure 6.

As the wall thickness decreases, the maximum *UxL* and *UyL* increase while the maximum *ML* decreases, and *Hv* is unaffected by the wall thickness. When *d* decrease from 120 to 40 cm, *UxL* and *UyL* increase from 17 to 26 cm and −1 to −8 cm, respectively, while *ML* decreases from 1,020 to 182 kNm. When existing structures exist, thicker walls should be built, and this thickness should be increased by the sensitivity of the existing structure.

Table 6 shows the analysis results performed at various *Df* to *He* ratios for *LS* and *DS* considering that the model size is 700 m horizontally and 350 m vertically and the mesh size is fine, $R_{\text{inter}} = 0.6$, $d = 40$ cm, and $B = 45$ m. The results include the maximum *Tst*, *UyL*, *UxL*, and *ML* values.

ML and *UxL* decrease significantly until the *Df* to *He* ratio is 1 while *Tst* remains almost unchanged, and no significant change is observed for larger ratios. Therefore, in the present study, the ratio of *Df* to *He* is assumed to be 1. As the *Df* decreases the *ML* increases and increasing the cross-

Table 4: The effects of the boundary conditions on the excavation model.

Boundaries (m)	Soil	*Tst* (kN)	*Hv* (mm)	*UyL* (mm)	*UxL* (mm)	*ML* (kNm)
$X=200$ $Y=100$	LS	896.31	142.50	−15.79	33.64	426.00
	DS	509.52	62.40	−12.50	17.34	173.70
$X=300$ $Y=150$	LS	888.07	156.20	−10.90	33.63	428.80
	DS	502.84	71.98	−7.98	17.21	178.80
$X=500$ $Y=250$	LS	883.39	167.50	−5.67	34.50	437.40
	DS	501.49	81.84	−3.87	17.28	181.40
$X=700$ Y = 350	LS	869.95	175.00	−4.02	37.10	456.40
	DS	506.17	87.21	−3.40	18.18	185.70
$X=900$ $Y=450$	LS	888.48	183.90	−4.64	40.11	476.00
	DS	491.85	90.69	−3.08	18.72	190.40
$X=1100$ $Y=550$	LS	887.93	186.10	−4.09	42.38	489.70
	DS	497.24	93.30	−2.83	19.78	200.00

Table 5: The effect of the mesh size on the excavation model.

Mesh	Soil	*Tst* (kN)	*UxL* (mm)	*UyL* (mm)	*ML* (kNm)	*Hv* (mm)
Very coarse	LS	843.17	72.80	−42.93	365.80	199.00
	DS	504.49	30.20	−9.29	255.90	88.72
Coarse	LS	815.31	65.06	−37.73	499.50	190.10
	DS	482.13	27.93	−8.19	209.10	88.37
Medium	LS	813.34	63.85	−37.46	477.90	186.40
	DS	465.53	26.90	−8.09	205.30	87.49
Fine	LS	815.23	60.67	−35.50	447.20	181.60
	DS	454.80	25.92	−8.73	185.70	87.43
Very fine	LS	806.23	60.18	−36.40	429.40	179.60
	DS	461.18	25.50	−9.20	182.80	87.19

section of the wall and consequently the cost. Simultaneously, due to the increase in the settlement of the soil behind the wall, the safety and usability of existing structures may be threatened. Therefore, determining the embedment depth considering both economy and safety is necessary for the *Df* values smaller than the *He*.

3.5. The Effect of the Coefficient of the Strength Reduction in the Interface. Table 7 shows the analysis results performed for different R_{inter} values for *LS* and *DS* considering that the model size is 700 m horizontally and 350 m vertically and the mesh size is fine, $d=40$ cm, $Df=16$ m, and $B=45$ m. The results include the maximum values for *Tst*, *UyL*, *UxL*, *ML*, and *Hv*.

As the R_{inter} increases, the maximum *UxL*, *UyL*, and *ML* in *LS* and *DS* decrease, whereas the maximum *Hv* for *DS* is hardly affected. Since the reduction is slight for values larger than 0.6, and the friction angle between the wall and the soil is usually assumed to be two-thirds of the internal friction angle in practice, R_{inter} is supposed to be 0.6 in the present study. The friction between the wall and the soil must be accurately measured and taken into account in the calculations because it can cause especially the deformation values to increase by up to 30%–40% in *UxL* and 300% in *UyL*.

3.6. The Effect of the Width of the Excavation Pit. The impact of the width of the excavation on the deformation and bending moment of the *WL* and the deformations behind the *WL* and at the bottom of the excavation considering that the model size is 700 m horizontally and 350 m vertically and the mesh size is fine, $d=40$ cm, $Df=16$ m, and $R_{\text{inter}}=0.6$ is shown in Figure 7.

UxL, *UyL*, *ML*, and *Hv* increase as the *B* increases and the point of maximum of *UxL* is moving away from the bottom of the excavation. When *B* increases from 5 to 45 m, maximum *UxL*, *UyL*, and *ML* increase from 10 to 25 cm and from −3 to −8 cm, and from 160 to 185 kNm, respectively. Because a rise in pit width causes significant increases in the horizontal displacement of the wall and soil settlement, it should be operated in as small apertures as feasible. When necessary, alternatives such as progressive excavation should be proposed while using extreme caution.

3.7. The Effects of the Surcharge Loads. The analyses are performed for the no surcharge case, the symmetric surcharge case, and the asymmetric surcharge case. In the loading cases of the symmetrical situation, there are 60, 45, 30, 20, and 10 kPa surcharge loads on both sides of the excavation. When determining these loads, it is assumed that a single-story building exerts pressure on the soil of around 10–15 kPa. Furthermore, because there will be existing buildings around the excavation, particularly in towns, and because they may have varying levels,

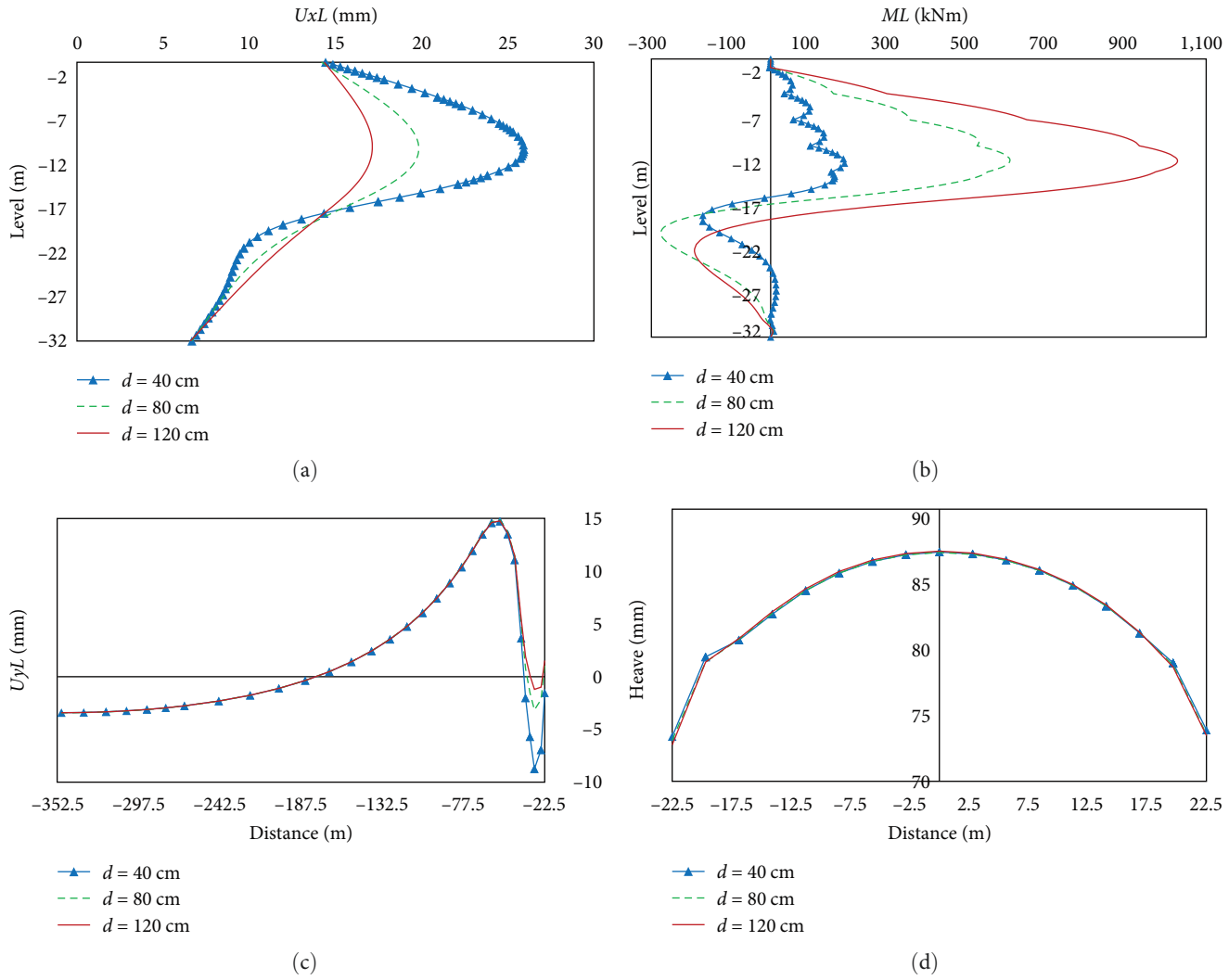

Figure 6: The effects of the thickness of the walls on (a) UxL, (b) ML, (c) UyL, and (d) Hv.

Table 6: The influence of the ratio of Df to He on the excavation model.

Df/He	Soil	*Tst* (kN)	*UxL* (mm)	*UyL* (mm)	*ML* (kNm)
0.25	LS	885.81	68.69	−49.31	607.10
	DS	505.33	25.66	−10.03	210.60
0.5	LS	846.26	63.23	−40.60	464.70
	DS	470.59	25.49	−9.26	183.20
1	LS	806.23	60.18	−36.40	429.40
	DS	461.18	25.50	−9.20	182.80
1.5	LS	806.38	59.13	−35.91	427.30
	DS	469.77	25.93	−10.16	179.30
2	LS	817.25	57.05	−33.97	423.50
	DS	472.32	25.93	−10.56	179.30

Table 7: The effect of R_{inter} on the excavation model.

R_{inter}	Soil	*Tst* (kN)	*UxL* (mm)	*UyL* (mm)	*Hv* (mm)	*ML* (kNm)
0.4	LS	845.96	72.37	−52.45	196.40	504.00
	DS	489.87	29.09	−11.97	88.56	215.30
0.6	LS	806.23	60.18	−36.40	179.60	429.40
	DS	461.18	25.50	−9.20	87.19	182.80
0.8	LS	778.37	53.74	−28.17	173.40	395.50
	DS	441.32	23.66	−7.25	86.28	206.30
1	LS	765.77	50.25	−24.51	171.40	402.10
	DS	438.62	22.92	−3.41	85.96	215.60

analyses were performed for equal and different surcharge load scenarios on both sides of the excavation. The asymmetric loading cases include cases where the surcharge load acting behind the *WL*, called *qL*, is kept constant at 60 kPa and the surcharge loads acting behind the wall on the excavation's right side (*qR*), are 45, 30, 20, 10, and 0 kPa. The analyses use Plaxis 2D v20, a finite element-based computer software. The *Tst*, deformations and bending moments on the walls, deformations on the soil surface, and the excavation pit are presented in the tables and figures. Later, using SPSS

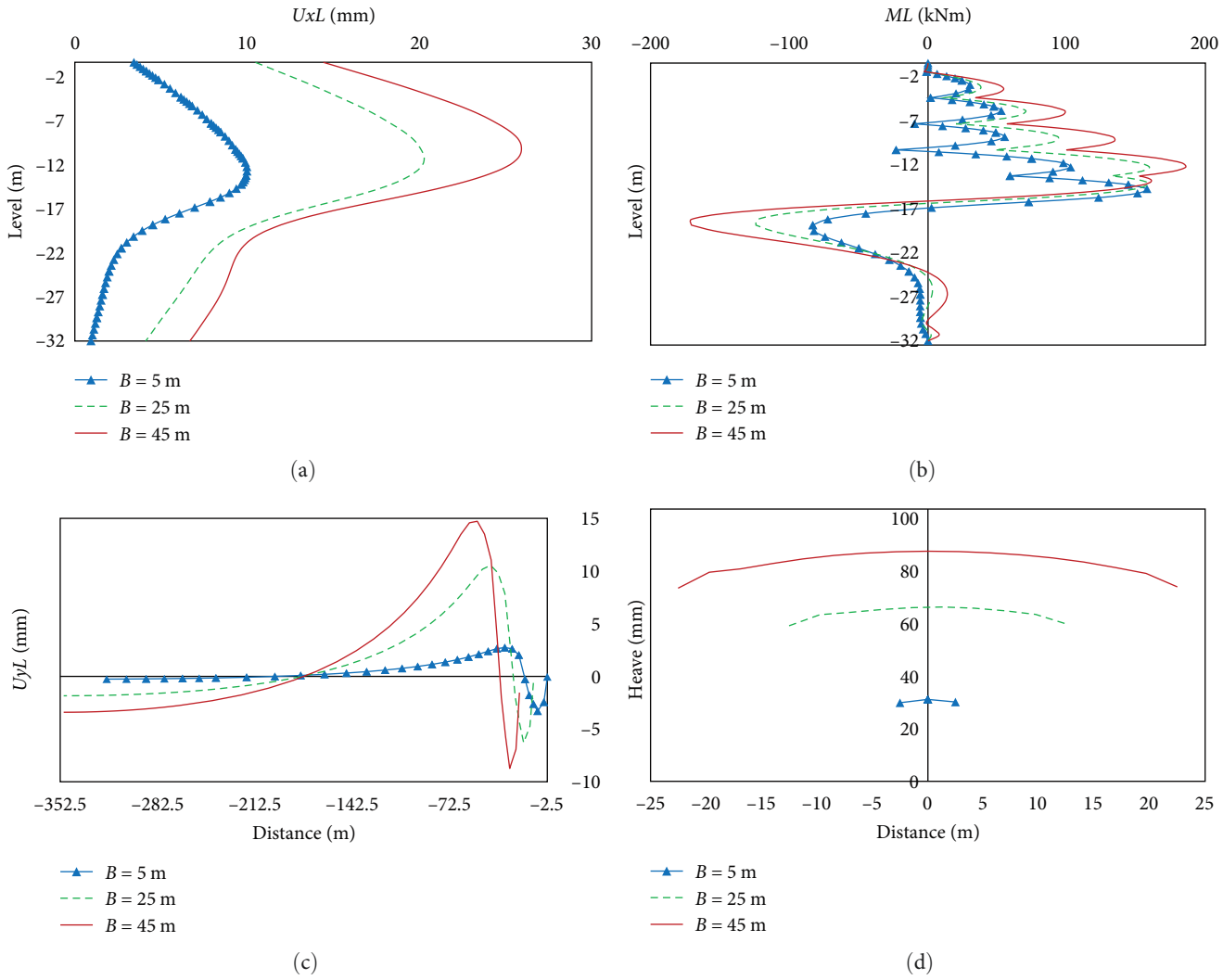

FIGURE 7: The effects of the width of the excavation on (a) UxL, (b) ML, (c) UyL, and (d) Hv.

Statistics v17 statistical software, linear and polynomial relationships are obtained, showing their variation as a function of surcharge loads.

3.8. The Effect of Surcharge Loads on the Strut Forces. Table 8 shows the maximum *Tst* results from the analysis performed for the different symmetrical and asymmetrical surcharge loading conditions for *LS* and *DS* considering that the model size is 700 m horizontally and 350 m vertically and the mesh size is fine, $d = 40$ cm, $R_{\text{inter}} = 0.6$, $Df = 16$ m, and $B = 45$ m. The maximum *Tst* increases with increasing surcharge load for both asymmetric and symmetric loading for *LS* and *DS*. The maximum *Tst* is 385, 453, and 506 kN respectively, when both sides are empty, one side is loaded with 60 kPa and the other is empty, and both sides are loaded at 60 kPa for *DS*.

Tstrut increases as the surcharge loads increase, and the asymmetry of the surcharge loads has no additional negative effects on the Tstrut for *LS* and *DS*. The maximum *Tst* values are almost twice as high for *LS* as for *DS*. In addition, the correlation between the maximum *Tst* and the surcharges can be expressed by Equations (1)–(3) for *LS* and Equations (4)–(6) for *DS*. It should be emphasized that these equations will only produce valid results for loose and dense sandy soils with the same or close values of wall and sturt properties employed in the present paper, and for surcharge loads of less than 60 kPa.

$$Tst = 3.1016 \text{ x } qL + 711.47 \; R^2 = 99.22 \text{ for } qL = qR, \tag{1}$$

$$Tst = 1.6527 \text{ x } qL + 718.29 \; R^2 = 99.46 \text{ for } qR = 0 \text{ kPa}, \tag{2}$$

$$Tst = 0.0189 \text{ x } (qR)^2 + 0.3197 \text{ x } qR + 813.55 \; R^2 = 99.6 \text{ for } qL = 60 \text{ kPa}, \tag{3}$$

$$Tst = 2.2816 \text{ x } qL + 367.35 \; R^2 = 99.89 \text{ for } qL = qR, \tag{4}$$

$$Tst = 1.432 \text{ x } qL + 364.73 \; R^2 = 99.12 \text{ for } qR = 0 \text{ kPa}, \tag{5}$$

Table 8: The maximum *Tst* values versus the surcharge loads *qL* and *qR*.

Soil	*qL* (kN/m)	*qR*	*Tst* (kN)	*qL* (kN/m)	*qR*	*Tst* (kN)
	10	0	732.12	10	10	746.33
	15	0	747.19	15	15	757.67
	20	0	752.84	20	20	766.21
	30	0	767.46	30	30	796.07
LS	45	0	794.45	45	45	856.67
	60	0	815.24	60	60	899.46
	60	45	869.28	60	15	822.46
	60	30	838.61	60	10	816.03
	60	20	828.43	0	0	716.21
	10	0	393.38	10	10	402.78
	15	0	397.51	15	15	414.54
	20	0	400.71	20	20	418.82
	30	0	414.17	30	30	434.07
DS	45	0	429.81	45	45	468.50
	60	0	453.68	60	60	506.22
	60	45	489.56	60	15	457.55
	60	30	474.89	60	10	458.71
	60	20	463.21	0	0	385.28

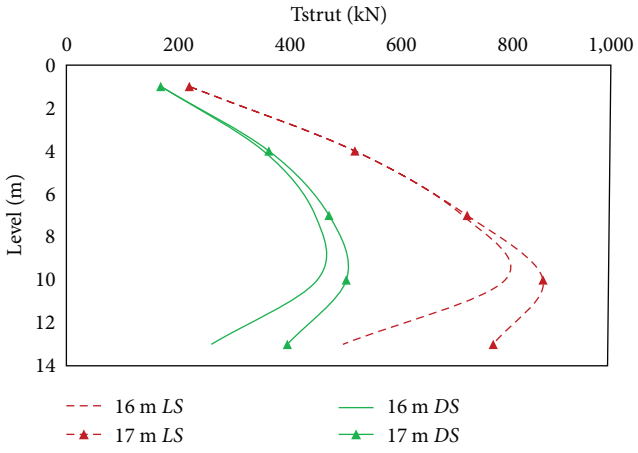

Figure 8: The Tst values for each strut in LS and DS for He = 16 m and He = 17 m.

$$Tst = 0.0086 \text{ x } (qR)^2 + 0.3886 \text{ x } qR + 453.21 \; R^2 = 98.91 \text{ for } qL = 60 \text{ kPa}. \quad (6)$$

The *Tst* increase with depth but decrease especially at the last strut, and the difference between the last two struts decreases as the distance between the previous strut and the bottom of the excavation changes from 3 to 4 m by increasing *He* to 17 m (Figure 8). This result is consistent with the approach that assumes the lateral earth pressure in braced excavations is trapezoidal. Another possible explanation is console-like behavior and a rapid decrease in wall lateral displacement toward the bottom.

3.9. The Effect of Surcharge Loads on the Lateral Deformations of the Walls. Table 9 shows the maximum *UxL* and *UxR* results from the analysis performed for the different symmetric and asymmetric surcharge conditions for *LS* and *DS* considering that the model size is 700 m horizontally and 350 m vertically and the mesh size is fine, $d = 40$ cm, $R_{inter} = 0.6$, $Df = 16$ m, and $B = 45$ m. The *UyL* values are almost twice as large in *LS* soils compared to *DS* soils for symmetrical load cases, but this difference gradually decreases as the surcharge load acting on *WR* decreases against a constant surcharge load on *LR*, and the asymmetry ratio increases.

The effects of surcharge loading with asymmetric conditions on lateral deformations at *WL* and *WR* along the walls for *DS* considering that the model size is 700 m horizontally and 350 m vertically and the mesh size is fine, $d = 40$ cm, $R_{inter} = 0.6$, $Df = 16$ m, and $B = 45$ m is shown in Figure 9. In the case of symmetrical loading, both *UxL* and *UxR* increase with the increase in surcharge load. However, in the case of asymmetric loading with a constant value of $qR = 0$ kPa, *UxL* increases while *UxR* decreases with the rise of *qL*. For an asymmetric load with a constant value of $qL = 60$ kPa, *UxL* decreases while *UxR* increases with the increase of *qR*. For symmetric conditions, the load increases the horizontal deformation of the wall, but while the asymmetry ratio increases because the load behind only one wall decreases, the deformation of the wall with decreasing load behind it decreases, whereas the deformation of the other wall increases even though the load behind it is constant. Therefore, when evaluating wall displacement, the influence of asymmetry, as well as the load, should be considered.

Except for a few cases for *WR*, less deformation occurred in asymmetric loading cases than in the unloaded case. It can be seen that the walls can affect each other positively and negatively through the struts. In addition, the correlation between the maximum *UxL* and *UxR* and surcharge loads can be expressed below in Equations (7)–(12) for *LS* and Equations (13)–(18) for *DS*. It should be emphasized that these equations will only produce valid results for loose and dense sandy soils with the same or close values of wall and sturt properties employed in the present paper, and for surcharge loads of less than 60 kPa.

$$UxL = 0.1224 \text{ x } qL + 32.894 \; R^2 = 99.9 \text{ for } qL = qR, \quad (7)$$

$$UxL = 0.438 \text{ x } qL + 33.08 \; R^2 = 99.72 \text{ for } qR = 0 \text{ kP}, \quad (8)$$

$$UxL = -0.2973 \text{ x } qR + 58.757 \; R^2 = 99.65 \text{ for } qL = 60 \text{ kPa}, \quad (9)$$

$$UxR = -0.1224 \text{ x } qL - 32.894 \; R^2 = 99.9 \text{ for } qL = qR, \quad (10)$$

$$UxR = 0.3122 \text{ x } qL - 32.57 \; R^2 = 99.69 \text{ for } qR = 0 \text{ kPa}, \quad (11)$$

Table 9: The maximum *UxL* and *UxR* values versus the surcharge loads.

Soil	*qL* (kN/m)	*qR*	*UxL* (mm)	*UxR* (mm)	*qL* (kN/m)	*qR*	*UxL* (mm)	*UxR* (mm)
	60	60	40.31	−40.33	45	0	53.40	−18.17
	60	45	45.64	−33.05	30	0	46.77	−22.69
	60	30	50.67	−26.21	20	0	42.00	−26.18
	60	20	53.14	−22.12	15	0	39.62	−27.89
LS	60	15	54.41	−20.18	10	0	37.13	−29.66
	60	10	55.86	−18.44	0	0	32.83	−32.82
	60	0	60.67	−14.36	20	20	35.41	−35.39
	45	45	38.25	−38.24	15	15	34.79	−34.77
	30	30	36.56	−36.54	10	10	34.13	−34.11
	60	60	18.80	−18.78	45	0	23.02	−13.50
	60	45	19.95	−17.31	30	0	20.52	−14.63
	60	30	21.92	−15.72	20	0	18.84	−15.37
	60	20	22.96	−14.70	15	0	18.36	−15.76
DS	60	15	23.57	−14.17	10	0	17.86	−16.13
	60	10	24.59	−13.42	0	0	16.88	−16.87
	60	0	25.92	−12.16	20	20	17.50	−17.50
	45	45	18.21	−18.20	15	15	17.44	−17.44
	30	30	17.74	−17.74	10	10	17.15	−17.15

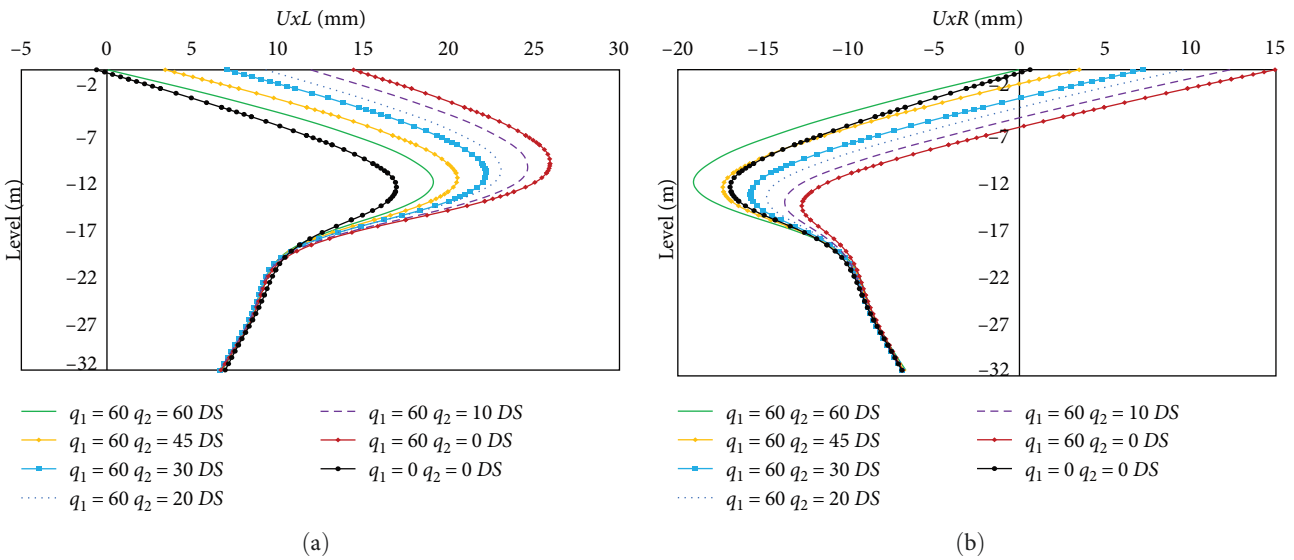

(a) (b)

Figure 9: The behavior of (a) UxL and (b) UxR along the walls for DS.

$$UxR = -0.4314 \text{ x } qR - 13.866 \; R^2 = 99.75 \text{ for } qL = 60 \text{ kPa}, \tag{12}$$

$$UxL = 0.0311 \text{ x } qL + 16.88 \; R^2 = 99.14 \text{ for } qL = qR, \tag{13}$$

$$UxL = 0.1723 \text{ x } qL + 15.408 \; R^2 = 99.88 \text{ for } qR = 0 \text{ kPa}, \tag{14}$$

$$UxL = -0.1279 \text{ x } qR + 25.733 \; R^2 = 99.59 \text{ for } qL = 60 \text{ kPa}, \tag{15}$$

$$UxR = -0.0308 \text{ x } qL - 16.879 \; R^2 = 99.15 \text{ for } qL = qR, \tag{16}$$

$$UxR = 0.0778 \text{ x } qL - 16.921 \; R^2 = 99.88 \text{ for } qR = 0 \text{ kPa}, \tag{17}$$

Table 10: The maximum *ML* and *MR* values versus the surcharge loads.

Soil	*qL* (kN/m)	*qR*	*ML* (kNm)	*MR* (kNm)	*qL* (kN/m)	*qR*	*ML* (kNm)	*MR* (kNm)
	10	0	417.70	417.40	10	10	423.30	423.20
	15	0	426.50	423.60	15	15	429.00	428.90
	20	0	429.10	425.20	20	20	431.10	431.10
	30	0	434.20	429.30	30	30	441.90	441.80
LS	45	0	441.20	436.70	45	45	456.70	456.60
	60	0	435.90	437.00	60	60	471.20	471.10
	60	45	462.10	464.70	60	15	445.70	445.20
	60	30	452.10	455.30	60	10	443.30	442.30
	60	20	446.90	447.60	0	0	410.70	410.70
	10	0	166.50	166.10	10	10	168.40	168.40
	15	0	168.20	167.60	15	15	171.40	171.40
	20	0	168.80	168.10	20	20	173.20	173.20
	30	0	173.30	171.30	30	30	178.50	178.50
DS	45	0	180.00	174.50	45	45	186.10	186.20
	60	0	180.50	157.00	60	60	193.80	193.90
	60	45	190.80	188.80	60	15	187.70	181.80
	60	30	189.40	185.50	60	10	185.40	179.90
	60	20	188.80	183.40	0	0	163.10	163.10

$$UxR = -0.1089 \text{ x } qR - 12.384 \; R^2 = 99.62 \text{ for } qL = 60 \text{ kPa}. \tag{18}$$

3.10. The Effect of Surcharge Loads on the Bending Moments of the Walls. Table 10 shows the maximum *ML* and *MR* results from the analysis performed for the different symmetric and asymmetric surcharge conditions for *LS* and *DS* considering that the model size is 700 m horizontally and 350 m vertically and the mesh size is fine, $d = 40$ cm, $R_{\text{inter}} = 0.6$, $Df = 16$ m, and $B = 45$ m. Figure 10 shows the effects of surcharge loading with asymmetric conditions on the bending moments at *WL* and *WR* along the walls for *DS*.

Both *ML* and *MR* increase with increasing surcharge load for both symmetric and asymmetric loading and it is more significant in *LS* compared to *DS*. In addition, the maximum values of *ML* and *MR* are more than twice as high at *LS* as at *DS*. Asymmetry in the loading causes an increase in the bending moment value for both walls as the asymmetry ratio increases. Even on the wall where the load does not change, the change in bending moment shows the interaction of both walls in braced systems and the importance of evaluating them together.

In addition, the correlation between the maximum *ML* and *MR* and surcharge loads can be expressed in Equations (19)–(24) for *LS* and Equations (25)–(30) for *DS*. It should be emphasized that these equations will only produce valid results for loose and dense sandy soils with the same or close values of wall and sturt properties employed in the present paper, and for surcharge loads of less than 60 kPa.

$$ML = 0.9859 \text{ x } qL + 412.35 \; R^2 = 99.67 \text{ for } qL = qR, \tag{19}$$

$$ML = -0.0041 \text{ x } (qL)^2 + 0.9024 \text{ x } qL + 411.18 \; R^2 = 98.16 \text{ for } qR = 0 \text{ kPa}, \tag{20}$$

$$ML = 0.4154 \text{ x } qR + 447.62 \; R^2 = 99.85 \text{ for } qL = 60 \text{ kPa}, \tag{21}$$

$$MR = 0.9859 \text{ x } qL + 412.35 \; R^2 = 99.67 \text{ for } qL = qR, \tag{22}$$

$$MR = -0.0073 \text{ x } (qL)^2 + 0.8891 \text{ x } qL + 410.44 \; R^2 = 98.84 \text{ for } qR = 0 \text{ kPa}, \tag{23}$$

$$MR = 0.5913 \text{ x } qR + 436.68 \; R^2 = 99.46 \text{ for } qL = 60 \text{ kPa}, \tag{24}$$

$$ML = 0.5082 \text{ x } qL + 163.29 \; R^2 = 99.95 \text{ for } qL = qR, \tag{25}$$

$$ML = 0.3751 \text{ x } qL + 162.5 \; R^2 = 99.33 \text{ for } qR = 0 \text{ kPa}, \tag{26}$$

$$ML = 0.1423 \text{ x } qR + 185.06 \; R^2 = 95.13 \text{ for } qL = 60 \text{ kPa}, \tag{27}$$

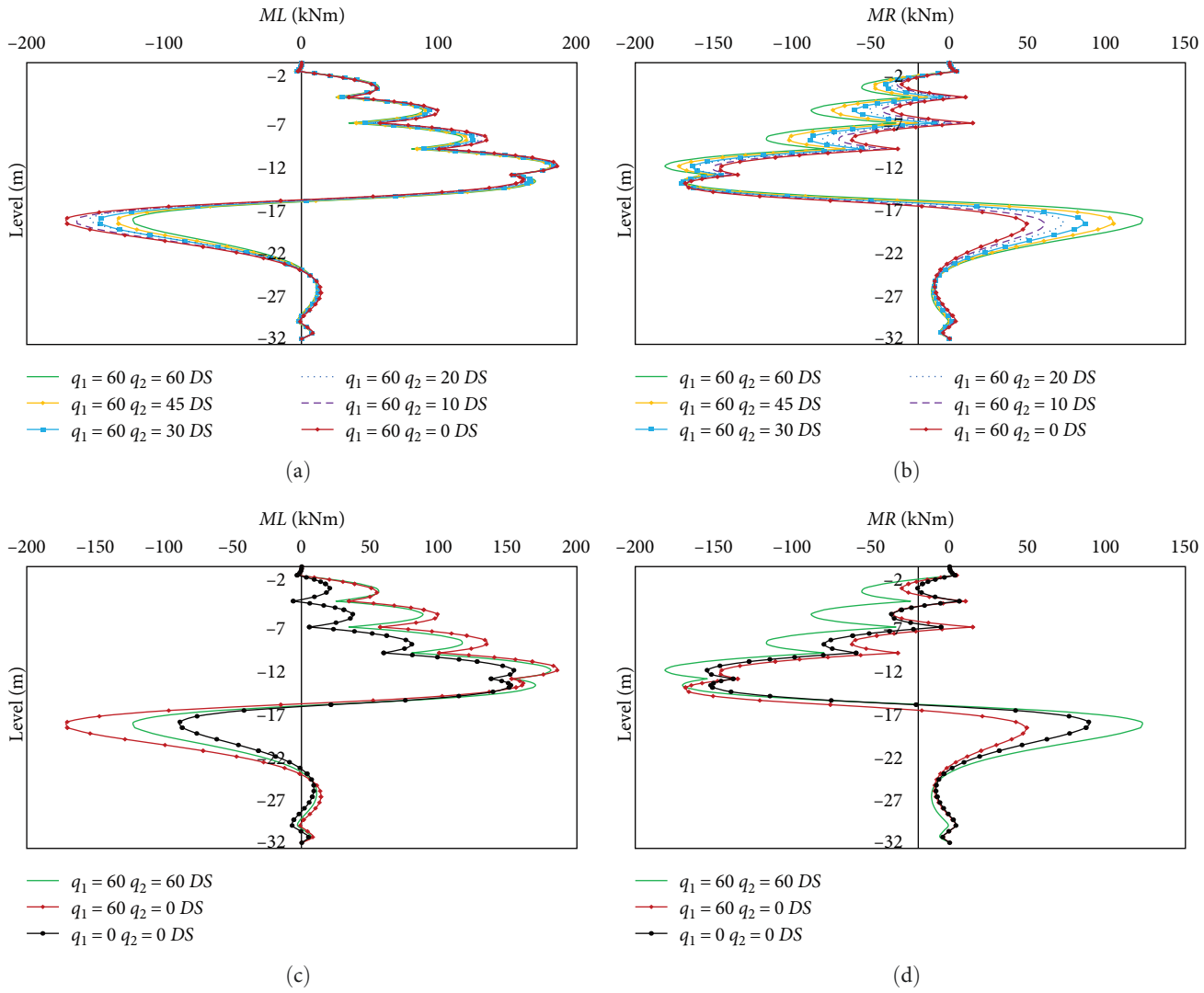

FIGURE 10: The behavior of (a and c) ML and (b and d) MR along the walls for DS.

$$MR = 0.5082\,\mathrm{x}\,qL + 163.30\ R^2 = 99.67 \text{ for } qL = qR, \tag{28}$$

$$MR = 0.2331\,\mathrm{x}\,qL + 163.69\ R^2 = 99.02 \text{ for } qR = 0\,\mathrm{kPa}, \tag{29}$$

$$MR = 0.2698\,\mathrm{x}\,qR + 177.4\ R^2 = 99.34 \text{ for } qL = 60\,\mathrm{kPa}. \tag{30}$$

3.11. The Effect of Surcharge Loads on the Surface Soil Settlements and Heaves. Table 11 shows the maximum *UyL* and *UyR* results for the different symmetric and asymmetric loading conditions for *LS* and *DS* considering that the model size is 700 m horizontally and 350 m vertically and the mesh size is fine, $d = 40$ cm, $R_{\text{inter}} = 0.6$, $Df = 16$ m, and $B = 45$ m. Also, Figure 11 shows the effects of surcharge loading with asymmetric conditions on the surface settlements behind the *WL* and *WR* along the walls for *DS*.

TABLE 11: The maximum *UyL* and *UyR* values versus the surcharge loads.

	qL (kN/m)	*qR* (kN/m)	*Uy* (mm) LS	*Uy* (mm) DS	*qL* (kN/m)	*qR* (kN/m)	*Uy* (mm) LS	*Uy* (mm) DS
UyL	60	60	−5.70	0.11	60	0	−35.50	−8.73
UyR			−5.69	0.15			26.64	11.93
UyL	60	45	−13.50	−1.87	45	0	−25.50	−4.54
UyR			5.34	2.97			22.15	10.83
UyL	60	30	−21.80	−4.07	30	0	−14.10	−1.12
UyR			14.22	5.89			18.57	9.26
UyL	60	20	−25.80	−5.05	20	0	−5.75	1.44
UyR			18.79	8.01			16.65	8.25
UyL	60	10	−29.50	−7.17	10	0	2.12	3.60
UyR			22.51	9.85			12.58	7.02
UyL	45	45	−2.01	1.64	20	20	3.30	3.83
UyR			−1.98	1.64			3.31	3.83
UyL	30	30	1.30	2.93	10	10	6.01	4.80
UyR			1.32	2.93			6.01	4.80

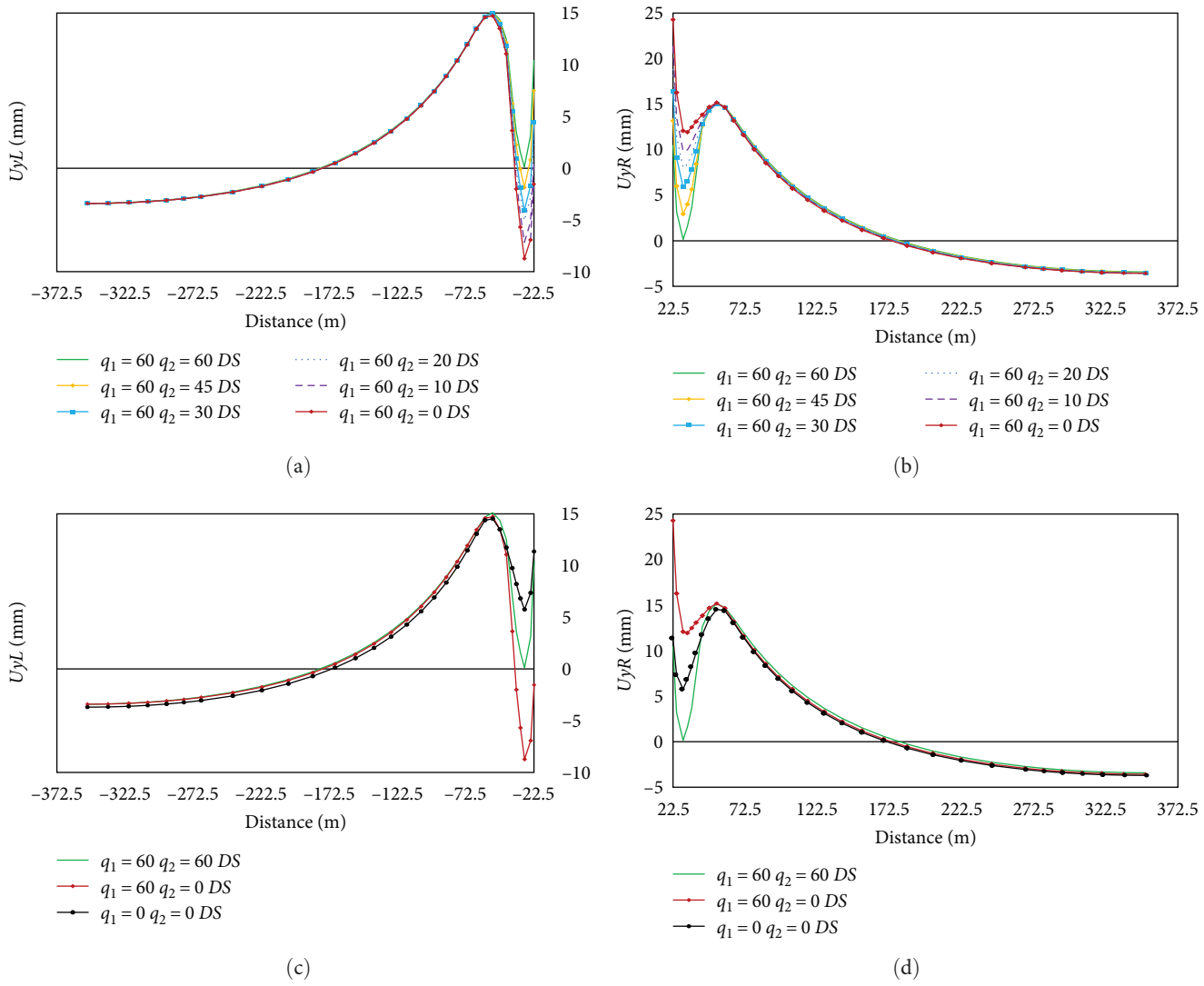

FIGURE 11: The behavior of (a and c) UyL and (b and d) UyR along the surface soil for DS.

While the asymmetry ratio increases because the surcharge load behind only one wall decreases, the deformation of the wall with decreasing load behind it decreases, whereas the deformation of the other wall increases even though the load behind it is constant. Therefore, when evaluating surface settlements, the influence of asymmetry, as well as the load, should be considered. Even on the wall where the load does not change, the change in surface settlements shows the interaction of both walls in braced systems and the importance of evaluating them together.

Furthermore, the correlation between maximum *UyL* and *UyR* and surcharge loads can be expressed in Equations (31)–(36) for *LS* and Equations (37)–(42) for *DS*. It should be emphasized that these equations will only produce valid results for loose and dense sandy soils with the same or close values of wall and sturt properties employed in the present paper, and for surcharge loads of less than 60 kPa.

$$UyL = -0.2342 \text{ x } qL + 8.354 \; R^2 = 99.85 \text{ for } qL = qR, \tag{31}$$

$$UyL = -0.7517 \text{ x } qL + 9.0583 \; R^2 = 99.87 \text{ for } qR = 0 \text{ kPa}, \tag{32}$$

$$UyL = 0.4862 \text{ x } qR - 35.346 \; R^2 = 99.6 \text{ for } qL = 60 \text{ kPa}, \tag{33}$$

$$UyR = -0.2342 \text{ x } qL + 8.354 \; R^2 = 99.85 \text{ for } qL = qR, \tag{34}$$

$$UyR = -0.2904 \text{ x } qL + 9.43228 \; R^2 = 99.36 \text{ for } qR = 0 \text{ kPa}, \tag{35}$$

Table 12: The maximum *Hv* values versus the surcharge loads.

qL (kN/m)	*qR*	*Hv* (mm) LS	*Hv* (mm) DS	*qL* (kN/m)	*qR*	*Hv* (mm) LS	*Hv* (mm) DS
60	60	175.00	87.38	60	0	179.6	87.43
60	45	176.20	87.41	45	0	177.2	87.37
60	30	177.40	87.43	30	0	174.6	87.36
60	20	178.3	87.38	20	0	173.00	87.34
60	10	179,00	87.44	10	0	172.2	87.34
45	45	174.00	87.34	20	20	172.8	87.36
30	30	173.40	87.34	10	10	172.2	87.35

$$UyR = -0.004\,\mathrm{x}\,(qR)^2 - 0.899\,\mathrm{x}\,qR + 26.311\ R^2 = 99.93 \text{ for } qL = 60\,\mathrm{kPa}, \tag{36}$$

$$UyL = -0.0929\,\mathrm{x}\,qL + 5.7371\ R^2 = 99.95 \text{ for } qL = qR, \tag{37}$$

$$UyL = -0.2406\,\mathrm{x}\,qL + 6.0158\ R^2 = 99.79 \text{ for } qR = 0\,\mathrm{kPa}, \tag{38}$$

$$UyL = 0.1466\,\mathrm{x}\,qR - 8.4961\ R^2 = 99.3 \text{ for } qL = 60\,\mathrm{kPa}, \tag{39}$$

$$UyL = -0.0929\,\mathrm{x}\,qL + 5.7372\ R^2 = 99.95 \text{ for } qL = qR, \tag{40}$$

$$UyR = 0.1033\,\mathrm{x}\,qL + 6.006\ R^2 = 99.2 \text{ for } qR = 0\,\mathrm{kPa}, \tag{41}$$

$$UyL = -0.1966\,\mathrm{x}\,qR + 11.878\ R^2 = 99.97 \text{ for } qL = 60\,\mathrm{kPa}. \tag{42}$$

Table 12 shows the maximum *Hv* for the different symmetrical and asymmetrical surcharge conditions for *LS* and *DS* considering that the model size is 700 m horizontally and 350 m vertically and the mesh size is fine, $d = 40$ cm, $R_{\text{inter}} = 0.6$, $Df = 16$ m, and $B = 45$ m. The maximum *Hv* values are not affected by the loading conditions and are almost twice as large for *LS* as for *DS*.

4. Conclusions

The current study intends to evaluate the link between surcharge loads and changes in strut loads, deformations, and bending moments on walls, soil surface settlements, and excavation heave in the deep excavations. Using PLAXIS 2D v20, a finite element-based computer program, deep excavation pits with diaphragm walls on loose (*LS*), and dense (*DS*) sandy soils are modeled for various symmetric and asymmetric loading scenarios. The maximum values of *Tst, UxL, UxR, ML, MR, UyL, and UyR* for both the left and right sides of the excavation, and the heaves (*Hv*) in the excavation are estimated using linear and polynomial second-order relationships using the SPSS Statistics v17 computer program.

The following conclusions were drawn from the study:

(i) With increasing surcharge load, both for *LS* and *DS*, under symmetric and asymmetric loading, the maximum of Tst rises.

(ii) Both *UxL* and *UxR* rise when the surcharge load increases in the case of symmetrical loading. In asymmetric loading, while the load on one side is constant, the increase in the load on the other side increases the deformation of the wall on the side where the load increases, while it reduces the deformation of the wall on the side where the load remains constant.

(iii) *ML* and *MR* increase with increasing surcharge load for both symmetrical and asymmetrical loading.

(iv) The maximum *Hv* values are unaffected by the loading conditions.

(v) The ground surface settlements increase as the surcharge load increase in symmetrical load scenarios. In asymmetrical loading scenarios, the swelling increase on the side on which the smaller load acts, whereas the settlement increases on the side which on the higher load as the asymmetry ratio increases.

(vi) The behavior of the retaining walls on the left and right sides are influenced by each other, therefore the strut-supported excavation systems should be designed as a whole, but not individually.

(vii) It should be emphasized that these equations only produce valid results for loose and dense sandy soils with the same or close values of wall and sturt properties employed in the present paper, and for surcharge loads of less than 60 kPa.

Consequently, it has been demonstrated that the estimating models produced by regression analyses and the outcomes from the finite element approach agree with one another. This gives promise that by broadening the study's scope in the future, viable models can be created using multiple regression analyses. All the results obtained are limited to the scope of the study, and it is necessary to continue and expand the studies to give more inclusive outcomes.

Data Availability

The data supporting the findings of this study are available within the article.

Conflicts of Interest

The author declares that there is no conflicts of interest.

References

[1] J. E. Bransby and G. W. E. Milligan, "Soil deformations near cantilever retaining walls," *Geotechnique*, vol. 24, pp. 175–195, 1975.

[2] C.-Y. Ou, P.-G. Hsieh, and D.-C. Chiou, "Characteristics of ground surface settlement during excavation," *Canadian Geotechnical Journal*, vol. 30, no. 5, pp. 758–767, 1993.

[3] G. W. Clough and T. D. O'Rouke, "Construction-induced movements of in situ walls," *Specialty Conference on Design and Performance of Earth Retaining Structures 1990*, pp. 439–470, 1990.

[4] K. Cheng, X. Riqing, H.-W. Ying, L. Cungang, and X. Gan, "Simplified method for calculating ground lateral displacement induced by foundation pit excavation," *Engineering Computations*, vol. 37, no. 7, pp. 2501–2516, 2020.

[5] I. H. Wong and A. T. C. Goh, "Performance of top–down basement excavation for the Singapore esplanade car park," *Journal of Southeast Asian Geotechnical Society*, pp. 49–59, 2009.

[6] M. Georgiadis and C. Anagnostopoulos, "Displacement of structures adjacent to cantilever sheet pile walls," *Soils and Foundations*, vol. 39, no. 2, pp. 99–104, 1999.

[7] T. Nakai, H. Kawano, K. Murata, M. Banno, and T. Hashimoto, "Model tests and numerical simulation of braced excavation in sandy ground: influences of construction history, wall friction, wall stiffness, strut position and strut stiffness," *Soils and Foundations*, vol. 39, no. 3, pp. 1–12, 1999.

[8] H.-P. Dang, H.-D. Lin, J. H. S. Kung, and C.-C. Wang, "Deformation behavior analyses of braced excavation considering adjacent structure by user-defined soil models," *Journal of GeoEngineering*, vol. 7, pp. 13–20, 2012.

[9] B.-C. B. Hsiung, "A case study on the behaviour of a deep excavation in sand," *Computers and Geotechnics*, vol. 36, no. 4, pp. 665–675, 2009.

[10] H. Peng, Q. Tang, L. Zhu, Z. Li, H. Li, and G. Wang, "Deformation control of subway stations under the influence of the construction of deep and large foundation pits with composite support systems," *Applied Sciences*, vol. 12, no. 6, Article ID 3026, 2022.

[11] F. Ghobrial, A. Fayed, M. Morsy, and M. Karray, "Numerical analysis of the effect of wall roughness in deep excavations in sand," *International Journal of Geotechnical Engineering*, vol. 5, no. 3, pp. 315–327, 2013.

[12] R. Peck, "Deep excavation and tunneling in soft ground," in *Proceedings of the 7th International Conference on Soil Mechanics and Foundation Engineering*, pp. 225–290, State-of-the-Art Report, Mexico, 1969.

[13] G. P. Tschebotarioff, *Soil Mechanics, Foundations, and Earth Structures*, McGrawHill Book Company Inc., New York, 2nd edition, 1973.

[14] S.-C. Hsu, Y.-P. Huang, and T.-M. Cheng, "Earth pressure distribution for deep excavations in gravel formations," in *Earthwork Project Management, Slope Stability Analysis, and Wave-Based Testing Techniques*, pp. 64–72, ASCE, 2014.

[15] K. Terzaghi and R. Peck, *Soil Mechanics in Engineering Practice*, John Wiley & Sons, Inc., New York, USA, 2nd edition, 1967.

[16] A. Debnath and S. K. Pal, "A numerical analysis on anchored sheet pile wall subjected to surcharge strip loading," *Journal of Engineering Research*, Article ID 100088, 2023.

[17] K. Fang, Z. Zhang, X. Liu, Q. Zhang, and C. Lin, "Numerical analysis of the behavior of special double-row support structure," *Journal of Civil Engineering and Management*, vol. 19, no. 2, pp. 169–176, 2013.

[18] A. Farag and A. Rashed, "Evaluation of ground movement induced by braced excavation using finite element analysis verified by case history," *Al-Azhar University Civil Engineering Research Magazine*, vol. 42, no. 1, pp. 69–78, 2020.

[19] Z. A. Hacheem, "Simulation of deep excavation in sand by finite element using hardening soil model (HSM)," *Engineering and Technology Journal*, vol. 29, no. 15, pp. 3079–3096, 2011.

[20] W. Hidayat, "Horizontal wall movement and ground surface settlement analysis of braced excavation based on support spacing," *UKaRsT*, vol. 5, no. 2, pp. 158–173, 2021.

[21] A. M. Hulagabali, P. Bariker, D. S. Gothakhindi, and C. H. Solanki, "Numerical study on prediction over behaviour of braced excavation in heterogeneous soil," in *Proceedings of Indian Geotechnical Conference 2020*, pp. 71–82, Andhra University, Visakhapatnam, 2020.

[22] H. Imtiaz, S. Naseer, Z. Khan, and H. Mahmood, "2D numerical analysis of deformations in diaphragm wall supported by horizontal struts," *International Journal of Civil & Structural Engineering*, vol. 6, no. 2, pp. 97–102, 2019.

[23] K. Liu, S. T. Ariaratnam, P. Zhang et al., "Mechanical response of diaphragm wall supporting deep launch shaft induced by braced excavation and pipe jacking operation," *Tunnelling and Underground Space Technology*, vol. 134, Article ID 104998, 2023.

[24] S. Mohamed, M. M. E. Zumrawi, and A. Ahmed, "Numerical analysis of deep excavation," *University of Khartoum Engineering Journal*, vol. 9, no. 1, pp. 47–51, 2019.

[25] A. Usmani, G. V. Ramana, and K. G. Sharma, "Analysis of braced excavation using hardening soil model," in *Proceedings of Indian Geotechnical Conference*, pp. 231–234, GEOtrentz, Mumbai, India, 2010.

[26] Y. Wang, J. Ouyang, P. Guo et al., "Performance of deep braced excavation under embankment surcharge load," *Geotechnical and Geological Engineering*, vol. 41, pp. 3575–3586, 2023.

[27] B.-C. B. Hsiung, K.-H. Yang, W. Aila, and C. Hung, "Three-dimensional effects of a deep excavation on wall deflections in loose to medium dense sands," *Computers and Geotechnics*, vol. 80, pp. 138–151, 2016.

[28] C. Chheng and S. Likitlersuang, "Underground excavation behaviour in Bangkok using three-dimensional finite element method," *Computers and Geotechnics*, vol. 95, pp. 68–81, 2018.

[29] A. T. C. Goh, F. Zhang, W. Zhang, Y. Zhang, and H. Liu, "A simple estimation model for 3D braced excavation wall deflection," *Computers and Geotechnics*, vol. 83, pp. 106–113, 2017.

[30] W. Zhang, Z. Hou, A. T. C. Goh, and R. Zhang, "Estimation of strut forces for braced excavation in granular soils from numerical analysis and case histories," *Computers and Geotechnics*, vol. 106, pp. 286–295, 2019.

[31] A. T. C. Goh and K. S. Wong, "Three-dimensional analysis of strut failure for braced excavations in clay," *Journal of Southeast Asian Geotechnical Society*, pp. 137–143, 2009.

[32] K. F. Pong, S. L. Foo, C. G. Chinnaswamy, C. C. D. Ng, and W. L. Chow, "Design considerations for one-strut failure according to TR26—a practical approach for practising engineers," *The IES Journal Part A: Civil & Structural Engineering*, vol. 5, no. 3, pp. 166–180, 2012.

[33] X. Wu, *Deformation Control Research on Deep Foundation Pit of Subway Transfer Station Paralleling with the Station Hall*, Tongji University of China, 2006.

[34] C. Xu, Y. Xu, H. Sun, and Q. Chen, "Characteristics of braced excavation under asymmetrical loads," *Mathematical Problems in Engineering*, vol. 2013, Article ID 452534, 12 pages, 2013.

[35] P. Guo, X. Gong, and Y. Wang, "Displacement and force analyses of braced structure of deep excavation considering unsymmetrical surcharge effect," *Computers and Geotechnics*, vol. 113, Article ID 103102, 2019.
[36] W. Zhang, N. Wu, P. Jia, X. Zhou, H. Li, and G. Wang, "Study of the mechanical performance of excavation under asymmetrical pressure and reinforcement measures," *Arabian Journal of Geosciences*, vol. 14, Article ID 1834, 2021.
[37] R. B. J. Brinkgreve, L. M. Zampich, and N. R. Manoj, PLAXIS 2D Connect Edition V20 manuals, 2019.
[38] R. B. J. Brinkgreve, E. Engin, and H. Engin, "Validation of empirical formulas to derive model parameters for sands," in *Numerical Methods in Geotechnical Engineering*, pp. 137–142, CRC Press, 2010.
[39] F. Xuan, *Behavior of Diaphragm Walls in Clays and Reliability Analysis*, Nanyang Technological University, Singapore, 2009.
[40] A. Goh, Z. Fan, L. Hanlong, Z. Wengang, and Z. Dong, "Numerical analysis on strut responses due to one-strut failure for braced excavation in clays," in *Proceedings of the 2nd International Symposium on Asia Urban GeoEngineering*, Springer Series in Geomechanics and Geoengineering, pp. 560–574, Springer, Singapore, 2018.